Supplement of Biogeosciences, 17, 813–831, 2020
https://doi.org/10.5194/bg-17-813-2020-supplement

Biogeosciences Open Access EGU

Supplement of

Trends and decadal oscillations of oxygen and nutrients at 50 to 300 m depth in the equatorial and North Pacific

Lothar Stramma et al.

Correspondence to: Lothar Stramma (lstramma@geomar.de)

Supplementary table

Table S1. Linear trends of solutes in µmol kg^{-1} yr^{-1} with 95% confidence intervals where data are available for the entire period since 1950, for negative (1950-1976; PDO-) and positive (after 1976; PDO+) PDO periods in the 50 to 300 m depth layer for April to December measurements for area P (48°-52°N, 143°-147°W) and Oyashio region (39°-42°N, 144°-149°E). Trends whose 95% confidence interval includes zero are shown in *italics*.

Parameter	trend	time period	PDO- trend	time period	PDO+ trend	time period
Area	area P		area P		area P	
Oxygen	*-0.22± 0.23*	1954-2017	*-0.16 ± 1.44*	1954-1976	*-0.22 ± 0.43*	1977-2017
Nitrate	+0.069 ± 0.050	1956-2017	*-0.114 ± 0.516*	1956-1973	+0.069 ± 0.050	1980-2017
Silicate	+0.491 ± 0.177	1958-2017	*+2.26 ± 5.74*	1958-1971	+0.216 ± 0.211	1987-2017
Phosphate	*+0.001 ± 0.003*	1954-2017	*-0.014 ± 0.025*	1954-1971	*+0.001 ± 0.007*	1980-2017
Area	Oyashio region		Oyashio region		Oyashio region	
Oxygen	*-0.18 ± 0.32*	1952-2017	*-0.27 ± 0.56*	1952-1976	*+0.14 ± 0.72*	1977-2017
Nitrate	+0.106 ± 0.043	1964-2017	*+0.365 ± 0.566*	1964-1976	+0.124 ± 0.060	1977-2017
Silicate	*+0.156 ± 0.340*	1952-2017	-1.40 ± 1.14	1952-1971	+0.614 ± 0.343	1981-2017
Phosphate	+0.006 ± 0.003	1953-2017	*+0.011 ± 0.017*	1953-1976	+0.009 ± 0.005	1977-2017

Supplementary figures

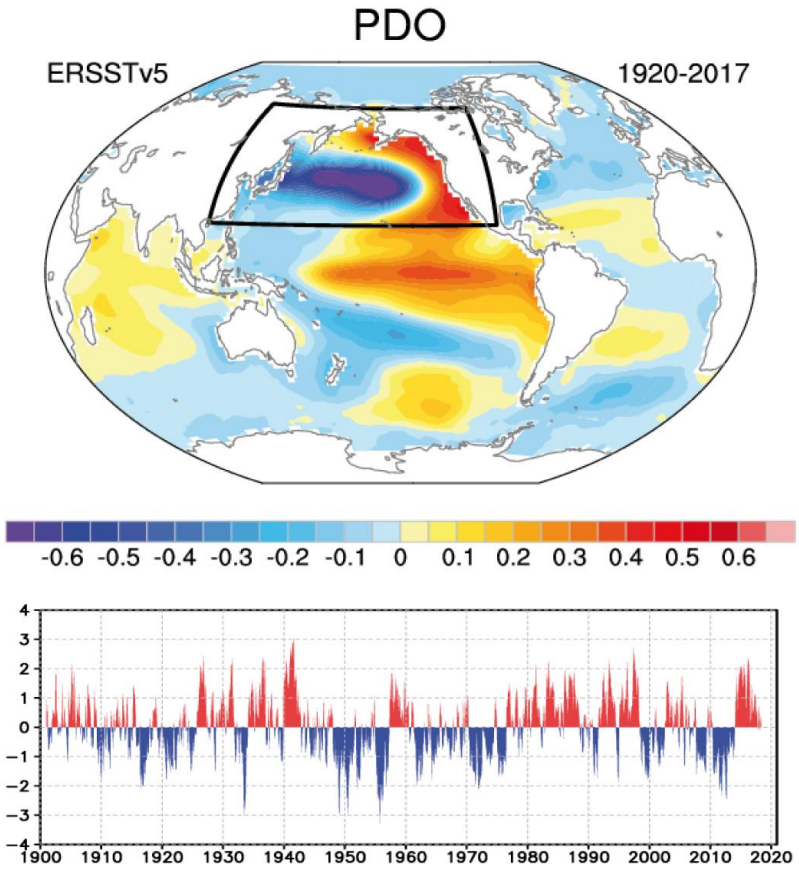

Figure S1. Global expression of the Pacific Decadal Oscillation (PDO, top) obtained by linearly regressing monthly sea surface temperature (SST) anomalies (in °C) based on ERSSTv5 data set (Huang et al., 2017) for the period 1920-2017 at each grid box upon the leading Principal Component (PC) time series based on the domain outlined in the black box (Adapted from Deser et al., 2010 and modified by A. Phillips). The PDO time series 1900 to 2017, defined by their corresponding PC is shown in the lower frame. (Figure from Tokyo Climate Center, http://ds.data.jma.go.jp/tcc/tcc/products/elnino/decadal/pdo_month.html) based on the HadlSST data set (Rayner et al., 2003).

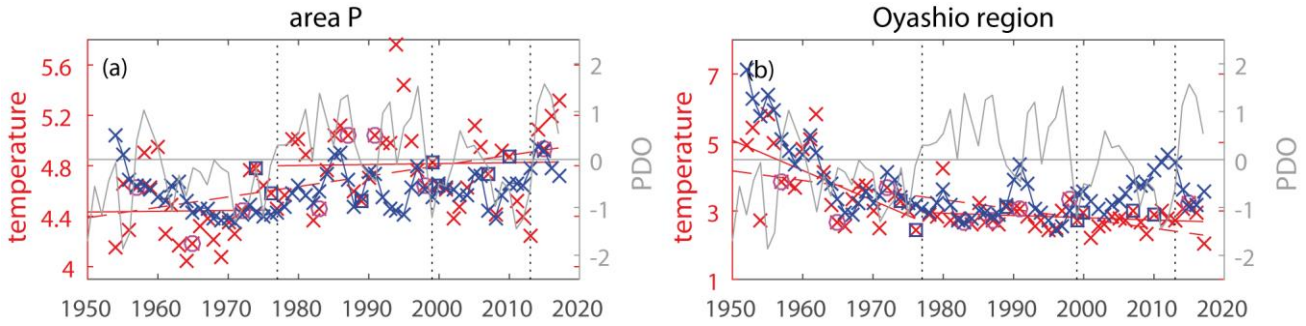

Figure S2. Annual mean temperature in °C for years available (red crosses) and trends for the layer 50 to 300 m plotted for the entire time period (dashed red lines) and for the periods 1950 to 1976 for the negative PDO phase and after 1976 for the positive PDO phase (solid red lines) a) at area P (48° to 52°N, 143° to 147°W) from hydrodata CTD and bottle data and station P data (50°N, 145°W) for the period 1954 to 2017 with a trend of 0.0083 +/- 0.0073 °C yr^{-1} and b) the Oyashio region between 39° and 42°N, 144° and 149°E for the period 1952 to 2017 with a trend of -0.0273+/-0.0188 °C yr^{-1}. El Niño years defined as strong are marked by an additional magenta circle, strong La Niña years by an additional blue square. The change of the PDO status in 1977, 1999 and 2013 are marked by vertical dotted lines. PDO annual time series are shown in the temperature time series as solid grey lines. In addition, the annual mean 0 to 50 m temperatures smoothed with a 4-point running mean are included as blue lines covering the temperature range 6.0 to 10.2 °C in area P and 5.3 to 16.4°C in the Oyashio region.

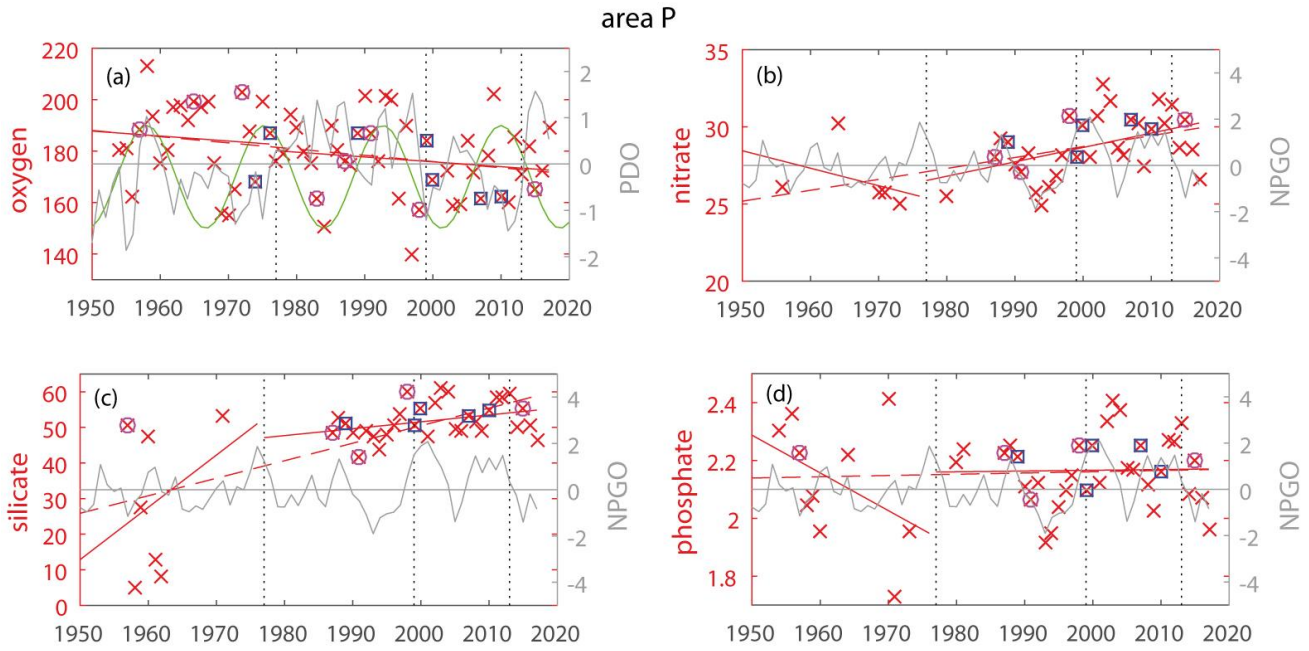

Figure S3. Annual mean concentration (in µmol kg^{-1}, red crosses) for years available and trends for the layer 50 to 300 m plotted for the entire time period (dashed red lines) and for the periods 1950 to 1976 for the negative PDO phase and after 1976 for the positive PDO phase (solid red lines) at area P (48° to 52°N, 143° to 147°W) from hydrodata CTD and bottle data and station P data (50°N, 145°W) for the period since 1956 in µmol kg^{-1} yr^{-1} for a) oxygen, b) nitrate, c) silicate and d) phosphate. For oxygen measurements in 2001 were removed as the 50-300 m mean was much to high (379 µmol kg^{-1}). El Niño years defined as strong are marked by an additional magenta circle, strong La Niña years by an additional blue square. The change of the PDO status in 1977, 1999 and 2013 are marked by vertical dotted lines. The PDO annual mean time series are shown in the oxygen time series and the NPGO annual mean time series in nitrate, phosphate and silicate time series as solid grey lines. In the oxygen time series the 18.6 year sinusoidal nodal cycle is included (green curve).

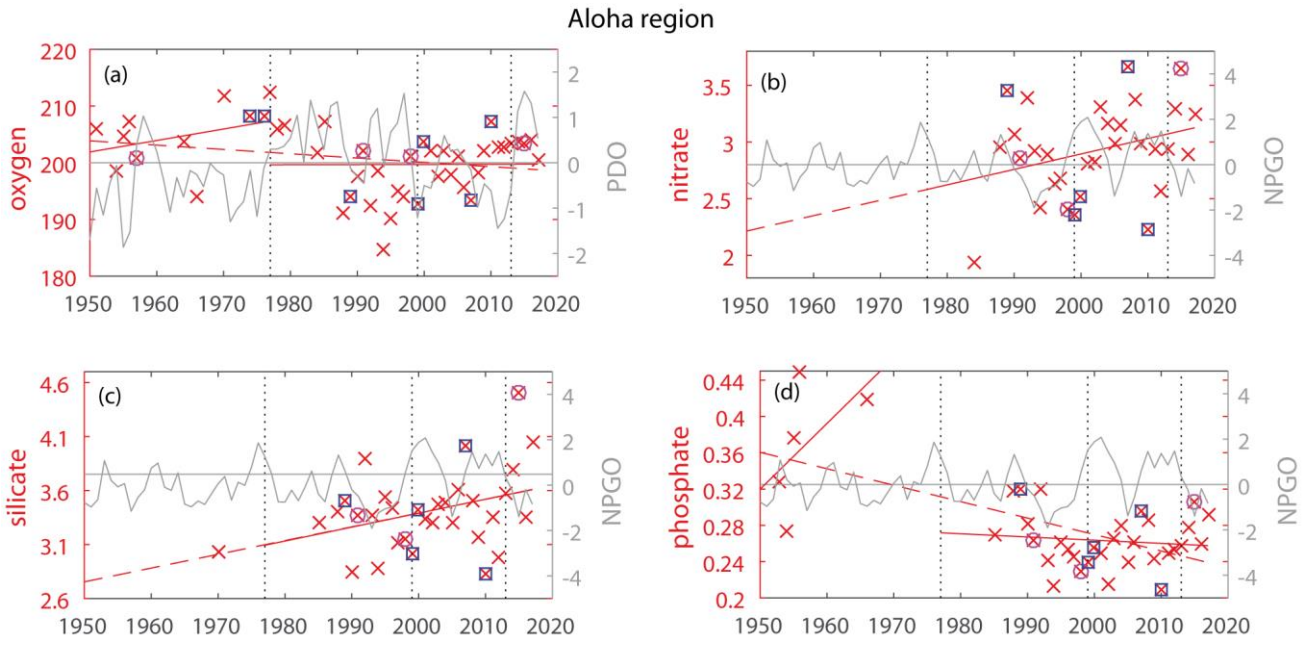

Figure S4. Annual mean concentration (in µmol kg^{-1}, red crosses) for years available and trends for the layer 50 to 300 m plotted for the entire time period (dashed red lines) and for the periods 1950 to 1976 for the negative PDO phase after 1976 for the positive PDO phase (solid red lines) between 22° and 25°N, 156 and 159°W from hydrodata CTD and bottle data and station Aloha data (22°45'N, 158°W) for the period since October 1988 in µmol kg^{-1} yr^{-1} for a) oxygen, b) nitrate, c) silicate and d) phosphate. For silicate measurements in 1984 were removed as they were to low (1.83 µmol kg^{-1}) phosphate measurements in 1951 were removed as the 50-300 m mean was to high (0.573 µmol kg^{-1}). El Niño years defined as strong are marked by an additional magenta circle, strong La Niña years by an additional blue square. The change of the PDO status in 1977, 1999 and 2013 are marked by vertical dotted lines. PDO annual mean time series are shown in the oxygen time series and the NPGO annual mean time series in nitrate, phosphate and silicate time series as solid grey lines.

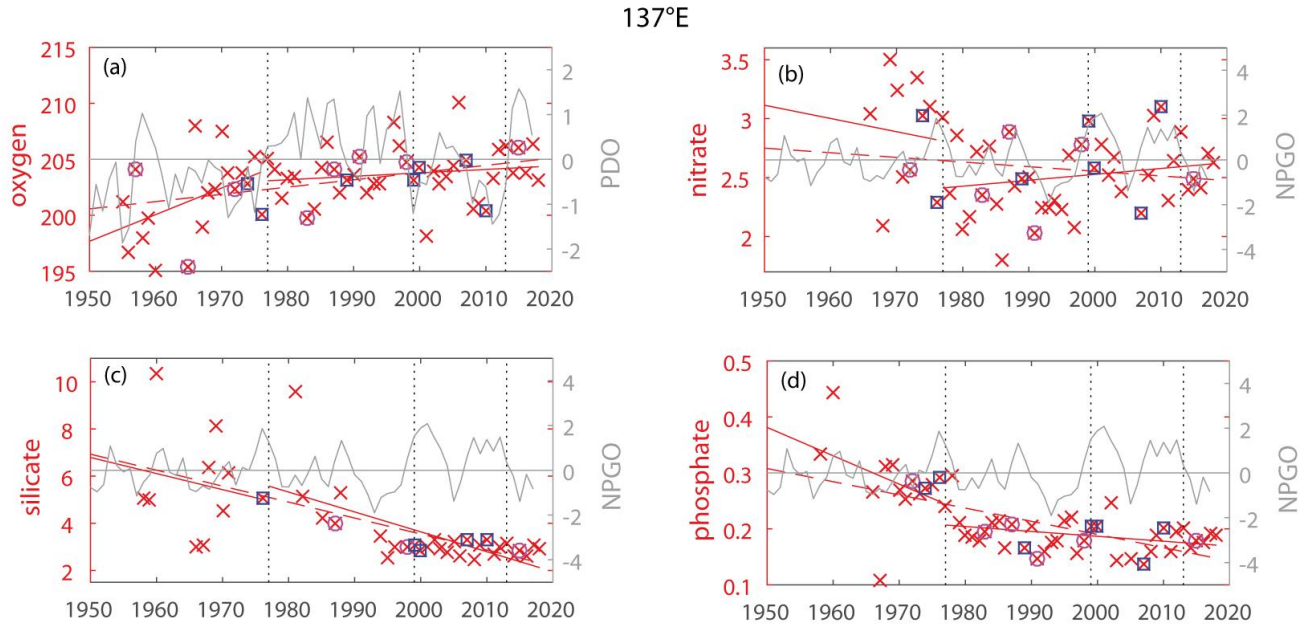

Figure S5. Annual mean concentration (in µmol kg^{-1}, red crosses) for years available and trends for the layer 50 to 300 m plotted for the entire time period (dashed red lines) and for the periods 1950 to 1976 for the negative PDO phase and after 1976 for the positive PDO phase (solid red lines) between 20° and 26°N, 134 and 140°E from hydrodata CTD and bottle data in µmol kg^{-1} yr^{-1} for a) oxygen, b) nitrate, c) silicate and d) phosphate. For oxygen measurements in 1982 and 1995 were removed as they were to high/low (1982: 236 µmol kg^{-1}, 1995: 185 µmol kg^{-1}), for nitrate 1959 was removed 14.4 µmol kg^{-1} and for silicate 1983 23.7 µmol kg^{-1}. El Niño years defined as strong are marked by an additional magenta circle, strong La Niña years by an additional blue square. The change of the PDO status in 1977, 1999 and 2013 are marked by vertical dotted lines. PDO annual mean time series are shown in the oxygen time series and the NPGO annual mean time series in the nitrate, silicate and phosphate time series as solid grey lines.

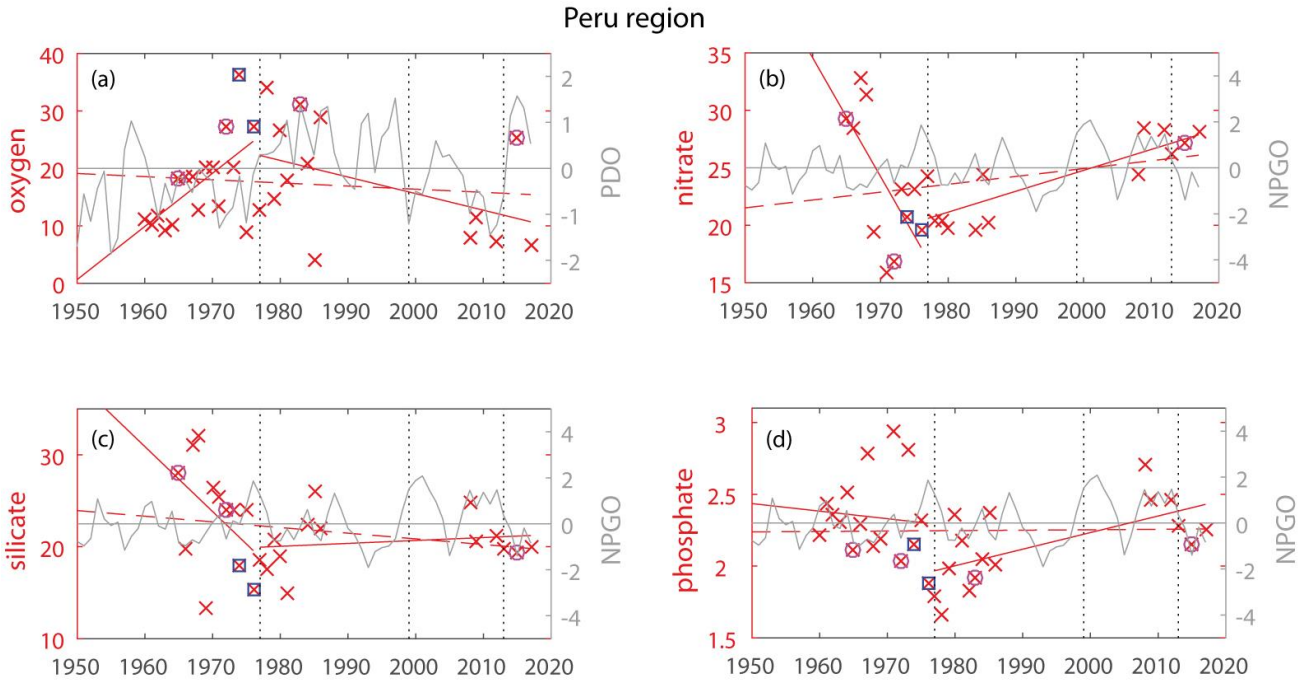

Figure S6. Annual mean concentration (in µmol kg^{-1}, red crosses) for years available and trends for the layer 50 to 300 m plotted for the entire time period (dashed red lines) and for the periods 1950 to 1976 for the negative PDO phase and after 1976 for the positive PDO phase (solid red lines) between 7° and 12°S, 78 and 83°W from hydrodata CTD and bottle data in µmol kg^{-1} yr^{-1} for a) oxygen, b) nitrate, c) silicate and d) phosphate. For oxygen measurements in 1982 were removed as they were to high (62.4 µmol kg^{-1}). El Niño years defined as strong are marked by an additional magenta circle, strong La Niña years by an additional blue square. The change of the PDO status in 1977, 1999 and 2013 are marked by vertical dotted lines. PDO annual mean time series are shown in the oxygen time series and the NPGO annual mean time series in the nitrate, silicate and phosphate time series as solid grey lines.

Supplementary references:

Deser, C., Alexander, M. A., Xie, S.-P., and Phillips, A. S.: Sea surface temperature variability: Patterns and mechanisms, Annu. Rev. Mar. Sci., 2, https.//doi.org/10.1146/annurev-marine-120408-151453, 2010.

Huang, B., Thorne, P. W., Banzon, V. F., Boyer, T., Cherupin, G., Lawrimore, J. H., Menne, M. J., Smith, T. M., Vose, R. S., and Zhang, H.-M.: Extended reconstructed sea surface temperature,

version 5 (ERSSTv5): Upgrades, validations, and intercomparisons, J. Climate, 30, https://doi.org/10.1175/JCLI-D-16-0836.1, 2017.

Rayner, N. A., Parker, D. E., Horton, E. B., Folland, C. K., Alexander, L. V., Rowell, D. P., Kent, E. C., and Kaplan, A.: Global analyses of sea surface temperature, sea ice, and night marine air temperature since the late nineteenth century, J. Geophys. Res. 108 D14, 4407, https://doi.org/10.1029/2002JD002670, 2003.